LETTER

doi:10.1038/nature12425

Measurement of a solid–state triple point at the metal–insulator transition in VO_2

Jae Hyung Park[1], Jim M. Coy[1], T. Serkan Kasirga[1], Chunming Huang[1], Zaiyao Fei[1], Scott Hunter[1] & David H. Cobden[1]

First-order phase transitions in solids are notoriously challenging to study. The combination of change in unit cell shape, long range of elastic distortion and flow of latent heat leads to large energy barriers resulting in domain structure, hysteresis and cracking. The situation is worse near a triple point, where more than two phases are involved. The well-known metal–insulator transition in vanadium dioxide[1], a popular candidate for ultrafast optical and electrical switching applications, is a case in point. Even though VO_2 is one of the simplest strongly correlated materials, experimental difficulties posed by the first-order nature of the metal–insulator transition as well as the involvement of at least two competing insulating phases have led to persistent controversy about its nature[1–4]. Here we show that studying single-crystal VO_2 nanobeams[5–16] in a purpose-built nanomechanical strain apparatus allows investigation of this prototypical phase transition with unprecedented control and precision. Our results include the striking finding that the triple point of the metallic phase and two insulating phases is at the transition temperature, $T_{tr} = T_c$, which we determine to be 65.0 ± 0.1 °C. The findings have profound implications for the mechanism of the metal–insulator transition in VO_2, but they also demonstrate the importance of this approach for mastering phase transitions in many other strongly correlated materials, such as manganites[17] and iron-based superconductors[18].

The metal–insulator transition (MIT) in VO_2 is accompanied by a large and rapid change in the conductivity and optical properties, with potential uses in switching and sensing. VO_2 has recently received renewed attention as a convenient strongly correlated material for the application of new ultrafast[19–21] and microscopy[22,23] techniques, ionic gating[24] and improved computational approaches[3,4]. However, the problems associated with bulk or film samples that consist of a complex of multiple solid phases and domains under highly non-uniform strain, as well as compositional variations such as oxygen vacancies[25] and hydrogen doping[26], make it almost impossible to disentangle the underlying parameters on which rigorous understanding can be built. The experiments described here eliminate these problems, allowing unprecedented control of the MIT and accurate determination of the underlying phase stability diagram of pure VO_2.

Figure 1a illustrates the structures of the phases involved in the MIT. In every phase there are two interpenetrating sets of parallel chains of vanadium atoms each surrounded by six oxygen atoms forming a distorted octahedron (the oxygen atoms are not shown). In the high-temperature metallic (rutile, R) phase all the chains are straight and periodic, whereas in the low-temperature insulating (monoclinic M1) phase every chain is dimerized. There are also two other known insulating phases: monoclinic M2, in which only one set of chains is dimerized, and triclinic T, which is intermediate between M1 and M2. The existence of both M1 and M2, with similar dielectric properties yet different magnetic properties, provides constraints on the theory of the MIT; for example, it rules out a purely Peierls-type mechanism[2]. In the older literature the MIT is taken to occur between R and M1, although recent studies[8–10,23] have shown that M2 domains occur in most VO_2 samples near the MIT, raising the question of its role in the transition.

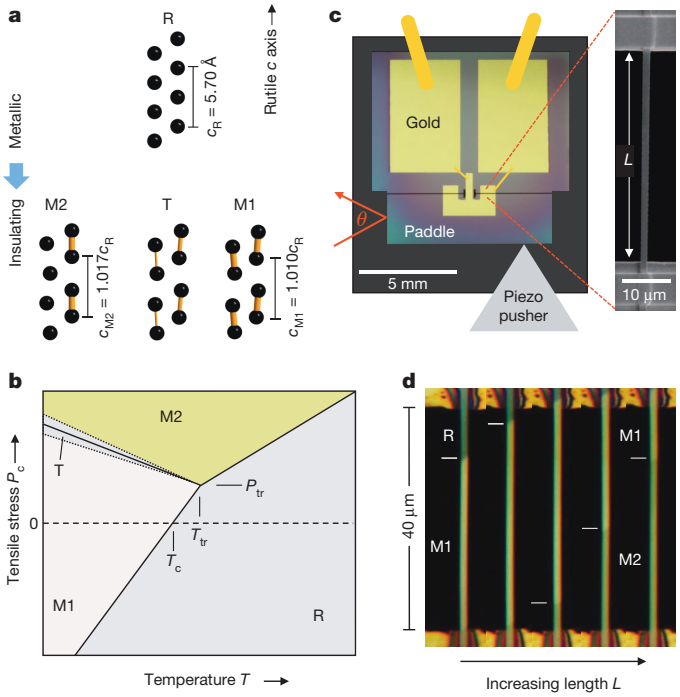

Figure 1 | Control of the metal–insulator transition in VO_2 using uniaxial stress. **a**, Arrangement of vanadium ions in the phases involved in the MIT, indicating their different vanadium chain periods and dimerization (yellow). **b**, Expected layout of the stress–temperature phase diagram near the MIT, showing the transition temperature T_c at zero stress. **c**, Experimental geometry, showing an electron micrograph (right) of a VO_2 nanobeam suspended across a slot of width L in a silicon chip (left, optical micrograph) whose width is controlled by pushing on the paddle and measured by deflection of a laser beam. The yellow lines signify gold wire bonds. **d**, Series of optical images showing movement of the R–M1 and M1–M2 interfaces as L is increased in roughly 100-nm steps at 64 °C (device P7, 40 μm gap).

The largest difference in unit cell shape between R, M1 and M2 is along the pseudo-rutile c axis (the vanadium chain axis), with c_R = 5.700 Å, c_{M1} = 5.755 Å and c_{M2} = 5.797 Å, as indicated in Fig. 1a. Compressive strain along this axis in an epitaxial film can lower the transition to room temperature[15,25]; thus, applying uniaxial tensile stress P_c along it can be used to control the transition[13,15]. A stability diagram in the P_c–T plane (with all other stress components zero) is expected to have the layout indicated in Fig. 1b. A shaded region indicates where the T phase occurs[7,27]. The effect of P_c on the phase stability (Fig. 1b) resembles that of stress along the $[110]_R$ axis[27] and of doping[28] by chromium. Rough ideas of the locations of the three phase boundaries have been obtained by modelling bent nanobeams[16]. The triple point (T_{tr}, P_{tr}) has not been located, although M1 and M2 are known to be very close in free energy near the transition[27]. The stress P_{tr} is normally taken to be positive, implying that a perfect unstrained crystal

[1]Department of Physics, University of Washington, Seattle, Washington 98195, USA.

shows a direct transition from M1 to R at T_c. We find that this is not in fact true, and T_{tr} is identical to T_c to within ± 0.05 °C, or one part in 10^4 in absolute temperature. We further determine T_c to be 65.0 ± 0.1 °C. In addition we present evidence that in the neighbourhood of T_c the M1 phase can distort continuously under tension into the metastable T phase. These discoveries have deep implications for the physics of the MIT, for the interpretation of many measurements on VO_2 crystals and films, and for mastering the transition with a view to applications.

Our investigations of the MIT rest on the ability to precisely control the length of a suspended single-domain nanobeam and thereby to apply pure uniaxial stress along it, a situation that cannot be achieved in larger crystals because of domain structure. The elements of the experiment are illustrated in Fig. 1c (see Methods). A VO_2 nanobeam is fixed, in some cases with electrical contacts, across a micromachined slot in a silicon chip whose width L can be varied with nanometre precision. We perform measurements only when the nanobeams are straight, so the maximum compressive stress is limited by buckling. By varying L and T, the three phases R, M1 and M2 can be induced and can be differentiated by reflection contrast with linearly polarized light[10], as illustrated in Fig. 1d, as well as by Raman spectroscopy[14] and measurements of electrical resistance. Linearly polarized light also reveals twinning[11], allowing us to select devices in which twinning is absent.

According to the phase diagram in Fig. 1b the state of the nanobeam as a function of L and T should include regions of two-phase coexistence as sketched in Fig. 2a. We find that the suspended part of the nanobeam can indeed be brought into coexistence between any pair of the three phases. The position of the interface changes smoothly and reproducibly with both L and T in between sudden reconfigurations. For the case of M2 + R coexistence we define the interface position y_{M2R} as the shift relative to an initial position such that it increases as R converts to M2. We define y_{M2M1} and y_{M1R} similarly.

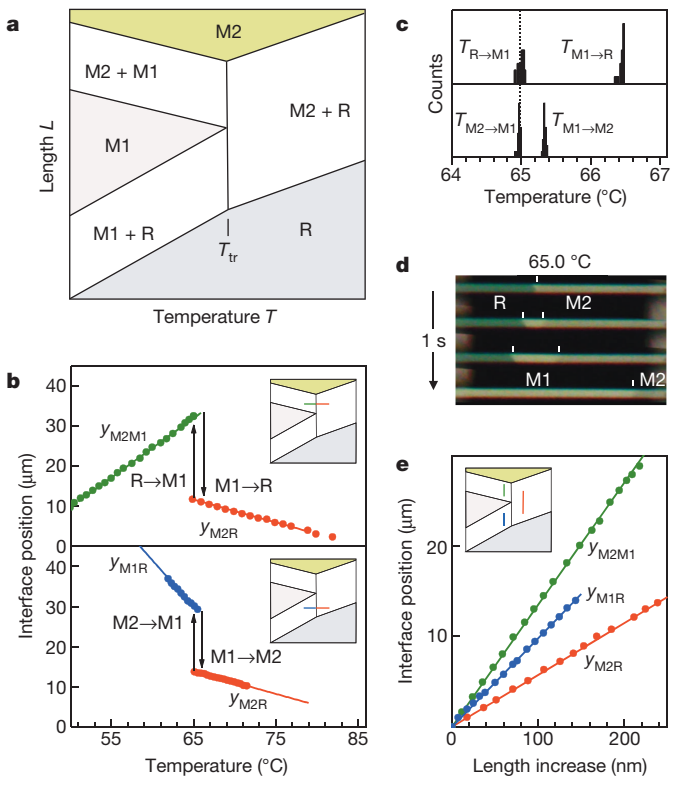

Figure 2 | Temperature and length dependence in coexistence. **a**, Expected configuration of a nanobeam as a function of T and L. **b**, Variation of interface positions with T at fixed L corresponding to moving along the lines in the insets (upper: device P11, 40 μm gap; lower: P9, 20 μm gap). Each interface type is indicated by a colour. **c**, Histograms of temperatures at which reconfigurations occur for 20 cycles sweeping at 0.1 °C min^{-1} (device P14, 40 μm). **d**, Sequence of images during reconfiguration from M2 + R to M2 + M1 in a nanobeam at the triple point, 65.0 °C (device P8B, 20 μm). **e**, Variation of interface positions with L at fixed T, corresponding to moving along the vertical lines in the inset (device P14). The fractional differences in lattice constants, α_{ij}, are the inverse slopes of these lines.

The MIT in VO_2 is usually studied as a function of T, without paying close attention to strain or to interconversion between M1 and M2. In undoped samples it is seen in the range 65–68 °C, with a hysteresis of several degrees Celsius, and the value of T_c is not known more precisely than this. In our experiments on nanobeams, as T is varied at fixed L we see the behaviour shown in Fig. 2b, which can be understood with reference to the colour-coded lines in the inset phase diagrams. If we start in M2 + M1 coexistence (Fig. 2b, upper panel, green) and increase T, the interface position y_{M2M1} first moves smoothly as the stress required for phase equilibrium changes[13]. Then at a temperature $T_{M1\to R}$ there is a sudden reconfiguration to M2 + R coexistence (Fig. 2b, upper panel, red) after which the interface position y_{M2R} moves smoothly again. On cooling, the reverse reconfiguration occurs at temperature $T_{R\to M1}$. Starting instead at a smaller length, in M1 + R coexistence (Fig. 2b, lower panel, blue), a jump to M2 + R coexistence (again red) occurs at $T_{M1\to M2}$, whereas the reverse occurs at $T_{M2\to M1}$. Histograms of the reconfiguration temperatures on repeated cycling at 0.1 °C min^{-1} are shown in Fig. 2c. For this device $T_{M1\to R}$ and $T_{M1\to M2}$ are narrowly peaked at 66.4 and 65.3 °C, respectively; for other devices different values are found. This can be explained by superheating of M1, which varies between devices because the ease of nucleation of the high-temperature phase (R or M2) depends on microscopic details.

In contrast, $T_{R\to M1}$ and $T_{M2\to M1}$ are both peaked at the same temperature, 65.0 °C, indicated by the dotted line in Fig. 2c. In several nanobeams of different sizes, grown on different occasions, these two temperatures always lay in the narrow range between 64.9 and 65.2 °C; moreover, neither storage in air for 6 months nor heating to 200 °C for 1 h changed them, indicating that effects of oxygen vacancies[25] and hydrogen doping[26] were minimal. This observation can be explained as follows. A small amount of M1 is often visible at the interface in M2 + R coexistence, probably because it reduces the elastic energy. On cooling there is therefore no need for nucleation of M1, and reconfiguration occurs as soon as the triple point is reached. In fact, the dynamics of this process can sometimes be observed. Figure 2d shows a sequence of images taken in less than a second during the reconfiguration of a nanobeam after bringing it slowly down to 65.0 °C in M2 + R coexistence. A small pre-existing wedge of M1 at the M2 + R interface rapidly expands to replace the R part of the nanobeam completely. All the above observations thus suggest that the triple point is between 64.9 and 65.2 °C.

We now consider varying L at fixed T. First, in coexistence between any pair of phases the interface position is linear in L, as shown in Fig. 2e. This follows from the fact that the interface moves so as to maintain P_c at the phase equilibrium value. A length increase δL causes an interface shift δy_{M1R}, which changes the natural length by δL to keep the strain constant. This implies that $\delta L = \alpha_{M1R}\delta y_{M1R}$, where $\alpha_{M1R} \equiv c_{M1}/c_R - 1$. Hence y_{M1R} should vary according to $dL/dy_{M1R} = \alpha_{M1R}$, and similarly $dL/dy_{M2M1} = \alpha_{M2M1} \equiv c_{M2}/c_{M1} - 1$ and $dL/dy_{M2R} = \alpha_{M2R} \equiv c_{M2}/c_R - 1 \approx \alpha_{M2M1} + \alpha_{M1R}$. Best linear fits to the data shown give $\alpha_{M2M1} = 0.0074$, $\alpha_{M1R} = 0.0100$ and $\alpha_{M2R} = 0.0174$, close to the values of 0.0073, 0.0098 and 0.0172 calculated from the known lattice constants[28,29].

The ability to control L allows us to confirm the temperature of the triple point and to determine the behaviour very close to it. We exploit the fact that the electrical resistance of the nanobeam, R_n, is sensitive to the phase composition because each phase has a different resistivity[12,13]. The measurements in Fig. 3 are for a device (P10) with indium contacts. Figure 3a shows that at 65.3 °C R_n changes smoothly with L, as a result of a smoothly changing M2 + R interface position for $T > T_{tr}$ (see inset, red line). In contrast, at 63.9 °C it changes in a more complicated way, reflecting the sequence M1 + R→M1→M2 + M1

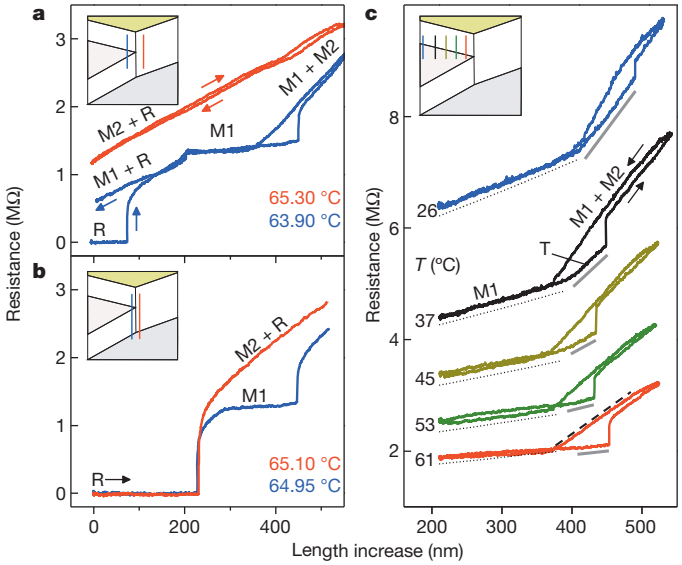

Figure 3 | Resistance–length measurements. **a**, At 65.3 °C, above the triple point (red line in inset), the resistance varies steadily in M2 + R coexistence. At 63.9 °C, below the triple point (blue line in inset), it reflects a sequence of transitions (device P10; L is varied at 8 nm s^{-1}). **b**, Starting in the R state, M2 nucleates if $T \geq 65.10$ °C (red), whereas M1 nucleates if $T \leq 64.95$ °C (blue), implying that these lie on either side of T_{tr} (see inset). **c**, The variation of the resistance with L and T is due to a strain-dependent activation energy in the M1 phase (dotted lines, offset by −0.15 MΩ for clarity) and to conversion of M1 to M2 in coexistence (dashed line). Grey lines indicate an additional resistance rise attributed to the T phase.

expected for $T < T_{tr}$ (see Fig. 3a inset, blue line). Jumps and hysteresis here show that M1 and M2 both require nucleation, which is consistent with the transitions being first order. To establish T_{tr} we measured R_n at a series of closely spaced temperatures, each time preparing the nanobeam in a fully metallic R state by cooling at sufficiently small L for R to be stabilized by compression, and then increasing L until an insulating domain nucleated. At 64.95 °C and below, the domain that appeared was always M1, whereas at 65.10 °C and above it was always M2, implying that T_{tr} was between these two values (see Fig. 3b). This is perfectly consistent with the range of T_{tr} deduced above from the T-sweeping measurements. Including uncertainties from variation between samples, temperature fluctuations and calibration, we conclude that $T_{tr} = 65.0 \pm 0.1$ °C.

Measurements of resistance versus length also yield other useful information, as illustrated in Fig. 3c (see Supplementary Information for details). First, the variation of the resistance of the M1 state with L and T is explained by a linear increase in the activation energy of the resistance with tensile strain $\eta = (L - L_0)/L_0$, L_0 being the effective natural length. The dotted lines are plots of $R_n \propto \exp[-(\Delta_0 + \gamma\eta)/k_BT]$ using coefficient values $\Delta_0 = 0.31$ eV and $\gamma = 0.77$ eV (the uncertainty in γ is 10%), where k_B is Boltzmann's constant. Second, from the variation of R_n in M1 + M2 coexistence (such as that indicated by the dashed line) we can deduce that $\rho_{M2}/\rho_{M1} = 2.3 \pm 0.2$ and that the activation energies of M1 and M2 are the same to within a few per cent. Third, a distinct additional increase in R_n, indicated by the solid grey lines, precedes the nucleation of M2 from M1. This can be explained by a continuous distortion of M1 into the T phase, which we immediately infer has a higher resistivity than M1 and is unstable relative to M2 at all temperatures from T_{tr} to below 26 °C.

Although we cannot measure the axial stress P_c directly, we can realize the condition $P_c = 0$ simply by breaking a nanobeam with a micromanipulator after other measurements have been completed. This produces opposing cantilevers, as illustrated in Fig. 4a. If the cantilevers are prepared in the fully M1 state by warming from lower temperature to around T_c and are then brought together, the compression produces a domain of R phase in one of them. After retraction, this domain persists only above a certain temperature, and shrinks and disappears below it. We identify this temperature with T_c, the transition temperature at zero stress. By performing the procedure on several devices we obtained the striking result that in every nanobeam T_c was equal to T_{tr}, to within an uncertainty of $\delta T \approx 0.05$ °C governed by temperature fluctuations. We thus conclude that $T_c = T_{tr} = 65.0 \pm 0.1$ °C.

Figure 4b shows the phase diagram of VO_2 inferred from measurements on ten nanobeams (see Supplementary Information for details). In brief, the $P_c(T)|_{ij}$ were deduced from measurements of y_{ij} ($i, j =$ M1, M2, R) versus T as follows. Because the stress in coexistence must take the phase equilibrium value, consideration of the variation of the

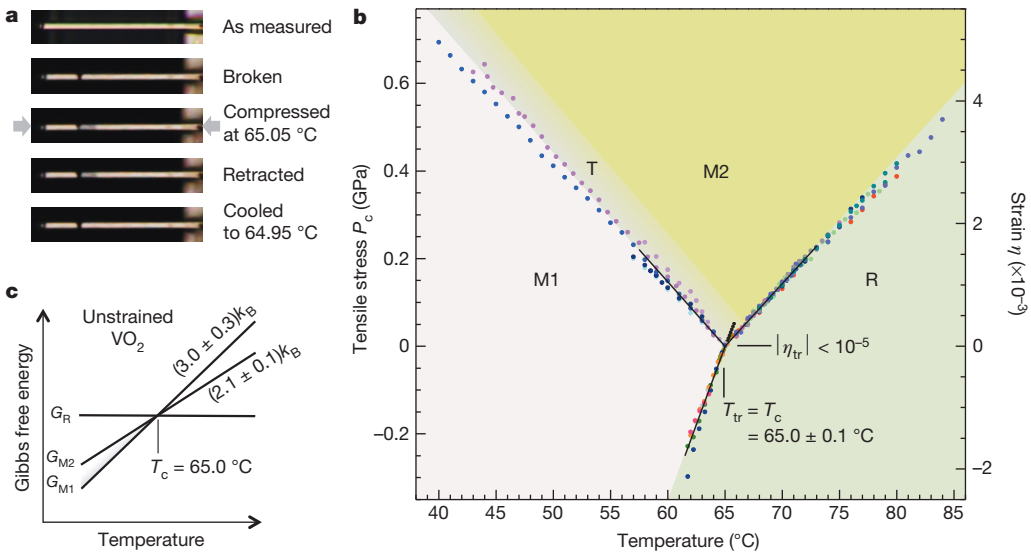

Figure 4 | Phase diagram of VO_2. **a**, The transition temperature T_c at zero stress is measured by finding the temperature above which the metallic phase (darker) becomes stable in a cantilever, as illustrated here (device P8). It is found to be equal to the triple point temperature: $T_c = T_{tr} = 65.0 \pm 0.1$ °C. **b**, Deduced stress–temperature phase diagram. The small black filled circles are for the superheated M1 phase. The grey shaded strip is where a metastable T phase can occur. **c**, The results imply that the free energies of all the phases are degenerate at T_c in unstrained pure VO_2.

strain $\eta = P_c/E$ with T (E is Young's modulus, taken to be 140 GPa for every phase[6]) yields[13]

$$\frac{1}{E}\frac{\partial P_c}{\partial T}\bigg|_{ij} = \frac{\mathrm{d}\eta}{\mathrm{d}T}\bigg|_{ij} = -\frac{\alpha_{ij}}{L_0}\frac{\mathrm{d}y_{ij}}{\mathrm{d}T} - \Delta K \quad (1)$$

The first term on the right is the change due to movement of the interface. The second, ΔK, is the thermal expansion mismatch between nanobeam and silicon substrate, which produces a correction of 5–10%. Given that $\eta(T_{tr}) = 0$, equation (1) can be used to derive $\eta(T)$ for each boundary. The deduced phase boundaries are straight, with uncertainties in their slopes of 5–10%, and obey the constraint at the triple point

$$\alpha_{M2M1}\frac{\mathrm{d}\eta}{\mathrm{d}T}\bigg|_{M2M1} + \alpha_{M1R}\frac{\mathrm{d}\eta}{\mathrm{d}T}\bigg|_{M1R} = \alpha_{M2R}\frac{\mathrm{d}\eta}{\mathrm{d}T}\bigg|_{M2R} \quad (2)$$

which is imposed by the Clausius–Clapeyron relations

$$\frac{\partial P_c}{\partial T}\bigg|_{ij} = \frac{S_j - S_i}{b^2(a_i - a_j)} \approx \frac{S_j - S_i}{\alpha_{ij} V} \quad (3)$$

in combination with equation (1). Here S_i is the entropy per vanadium pair in phase i, $b = 4.55$ Å is the base length of the rutile unit cell, and $V = 59$ Å^3 is the rutile unit cell volume. The value of $\partial P_c/\partial T|_{M1R} = 71$ MPa °C^{-1} corresponds to the known latent heat[30] of 1,020 cal per mole formula unit; $\partial P_c/\partial T|_{M2R} = 29$ MPa °C^{-1} corresponds to 710 cal mol^{-1}; and $\partial P_c/\partial T|_{M2M1} = -29$ MPa °C^{-1}. From the results we deduce entropy differences $S_R - S_{M1} = (3.0 \pm 0.3)k_B$ and $S_R - S_{M2} = (2.1 \pm 0.1)k_B$. The equality of T_{tr} and T_c to within $\delta T \approx 0.05$ °C implies that the strain η_{tr} at the triple point is smaller than $\delta T \mathrm{d}\eta/\mathrm{d}T|_{M2R} = 1.0 \times 10^{-5}$, where $\mathrm{d}\eta/\mathrm{d}T|_{M2R} = 2.0 \times 10^{-4}$ °C^{-1}, and this is also indicated on the phase diagram. Finally, the finding that the T phase is metastable with respect to M2 is indicated by a grey shaded strip within the M2 stability region.

To stress the implication of these results we sketch in Fig. 4c the T dependence of the Gibbs free energies G_i of the phases of unstrained VO_2, setting $G_R = 0$. The slopes are the entropies $S_i = -\mathrm{d}G_i/\mathrm{d}T$ at zero stress. Precisely at the MIT the insulating M1 and M2 phases are simultaneously degenerate with the metallic R phase. This and other facts revealed by our measurements are not explained by current models of the transition, but will be crucial ingredients of the correct theory. For example, further development and application of the Landau theory[10] of VO_2 should be prompted by our results. The insights we have gained into this important solid-state phase transition will be critical for both understanding and mastering the MIT in VO_2.

METHODS SUMMARY

VO_2 nanobeams grown by physical vapour transport were transferred onto slots on the micromachined silicon chips by using a micromanipulator and bonded with ultraviolet-curable epoxy (see Supplementary Information). Measurements from ten devices were used, and the temperature was calibrated with the known melting points of gallium and potassium (Supplementary Information). The slot width L (20 or 40 μm) was varied piezoelectrically on a temperature stage under an optical microscope (Supplementary Information).

Online Content Any additional Methods, Extended Data display items and Source Data are available in the online version of the paper; references unique to these sections appear only in the online paper.

Received 12 April; accepted 24 June 2013.

1. Zylbersztejn, A. & Mott, N. F. Metal–insulator transition in vanadium dioxide. *Phys. Rev. B* **11,** 4383–4395 (1975).
2. Rice, T. M., Launois, H. & Pouget, J. P. Comment on 'VO_2: Peierls or Mott–Hubbard? A view from band theory'. *Phys. Rev. Lett.* **73,** 3042 (1994).
3. Biermann, S., Poteryaev, A., Lichtenstein, A. I. & Georges, A. Dynamical singlets and correlation-assisted Peierls transition in VO_2. *Phys. Rev. Lett.* **94,** 026404 (2005).
4. Eyert, V. VO_2: a novel view from band theory. *Phys. Rev. Lett.* **107,** 016401 (2011).
5. Wu, J. Q. *et al.* Strain-induced self organization of metal–insulator domains in single-crystalline VO_2 nanobeams. *Nano Lett.* **6,** 2313–2317 (2006).
6. Guo, H. *et al.* Mechanics and dynamics of the strain-induced M1–M2 structural phase transition in individual VO_2 nanowires. *Nano Lett.* **11,** 3207–3213 (2011).
7. Atkin, J. M. *et al.* Strain and temperature dependence of the insulating phases of VO_2 near the metal–insulator transition. *Phys. Rev. B* **85,** 020101(R) (2012).
8. Sohn, J. I. *et al.* Surface-stress-induced Mott transition and nature of associated spatial phase transition in single crystalline VO_2 nanowires. *Nano Lett.* **9,** 3392–3397 (2009).
9. Zhang, S. X., Chou, J. Y. & Lauhon, L. J. Direct correlation of structural domain formation with the metal insulator transition in a VO_2 nanobeam. *Nano Lett.* **9,** 4527–4532 (2009).
10. Tselev, A. *et al.* Symmetry relationship and strain-induced transitions between insulating M1 and M2 and metallic R phases of vanadium dioxide. *Nano Lett.* **10,** 4409–4416 (2010).
11. Tselev, A. *et al.* Interplay between ferroelastic and metal–insulator phase transitions in strained quasi-two-dimensional VO_2 nanoplatelets. *Nano Lett.* **10,** 2003–2011 (2010).
12. Cao, J. *et al.* Constant threshold resistivity in the metal–insulator transition of VO_2. *Phys. Rev. B* **82,** 241101(R) (2010).
13. Wei, J., Wang, Z. H., Chen, W. & Cobden, D. H. New aspects of the metal–insulator transition in single-domain vanadium dioxide nanobeams. *Nature Nanotechnol.* **4,** 420–424 (2009).
14. Kasirga, T. S. *et al.* Photoresponse of a strongly correlated material determined by scanning photocurrent microscopy. *Nature Nanotechnol.* **7,** 723–727 (2012).
15. Cao, J. *et al.* Strain engineering and one-dimensional organization of metal–insulator domains in single-crystal vanadium dioxide beams. *Nature Nanotechnol.* **4,** 732–737 (2009).
16. Cao, J. *et al.* Extended mapping and exploration of the vanadium dioxide stress–temperature phase diagram. *Nano Lett.* **10,** 2667–2673 (2010).
17. Podzorov, V., Kim, B. G., Kiryukhin, V., Gershenson, M. E. & Cheong, S. W. Martensitic accommodation strain and the metal–insulator transition in manganites. *Phys. Rev. B* **64,** 140406(R) (2001).
18. Chu, J.-H., Kuo, H.-H., Analytis, J. G. & Fisher, I. R. Divergent nematic susceptibility in an iron arsenide superconductor. *Science* **337,** 710–712 (2012).
19. Becker, M. F., Buckman, A. B. & Walser, R. M. Femtosecond laser excitation of the semiconductor–metal phase transition in VO_2. *Appl. Phys. Lett.* **65,** 1507–1509 (1994).
20. Hilton, D. J. *et al.* Enhanced photosusceptibility near T_c for the light-induced insulator-to-metal phase transition in vanadium dioxide. *Phys. Rev. Lett.* **99,** 226401 (2007).
21. Kubler, C. *et al.* Coherent structural dynamics and electronic correlations during an ultrafast insulator-to-metal phase transition in VO_2. *Phys. Rev. Lett.* **99,** 116401 (2007).
22. Qazilbash, M. M. *et al.* Mott transition in VO_2 revealed by infrared spectroscopy and nano-imaging. *Science* **318,** 1750–1753 (2007).
23. Jones, A. C., Berweger, S., Wei, J., Cobden, D. & Raschke, M. B. Nano-optical investigations of the metal–insulator phase behavior of individual VO_2 microcrystals. *Nano Lett.* **10,** 1574–1581 (2010).
24. Nakano, M. *et al.* Collective bulk carrier delocalization driven by electrostatic surface charge accumulation. *Nature* **487,** 459–462 (2012).
25. Jeong, J. *et al.* Suppression of metal–insulator transition in VO_2 by electric field–induced oxygen vacancy formation. *Science* **339,** 1402–1405 (2013).
26. Wei, J., Ji, H., Guo, W. H., Nevidomskyy, A. H. & Natelson, D. Hydrogen stabilization of metallic vanadium dioxide in single-crystal nanobeams. *Nature Nanotechnol.* **7,** 357–362 (2012).
27. Pouget, J. P., Launois, H., Dhaenens, J. P., Merenda, P. & Rice, T. M. Electron localization induced by uniaxial stress in pure VO_2. *Phys. Rev. Lett.* **35,** 873–875 (1975).
28. Marezio, M., McWhan, B., Dernier, P. D. & Remeika, J. P. Structural aspects of metal–insulator transitions in Cr-doped VO_2. *Phys. Rev. B* **5,** 2541–2551 (1972).
29. Kucharczyk, D. & Niklewski, T. Accurate X-ray determination of the lattice parameters and the thermal expansion coefficients of VO_2 near the transition temperature. *J. Appl. Crystallogr.* **12,** 370–373 (1979).
30. Berglund, C. N. & Guggenheim, H. J. Electronic properties of VO_2 near the semiconductor–metal transition. *Phys. Rev.* **185,** 1022–1033 (1969).

Supplementary Information is available in the online version of the paper.

Acknowledgements We thank B. Spivak, A. Levanyuk and J. Wei for discussions. The silicon chips were patterned at the University of Washington Microfabrication Facility and the Nanofabrication Facility at the University of California, Santa Barbara. This work was supported by the US Department of Energy, Office of Basic Energy Sciences, Division of Materials Sciences and Engineering, award DE-SC0002197.

Author Contributions All authors performed measurements and device fabrication. J.H.P. and J.M.C. designed and constructed the apparatus. D.H.C. conceived and directed the experiments. D.H.C. and J.H.P. wrote the paper.

Author Information Reprints and permissions information is available at www.nature.com/reprints. The authors declare no competing financial interests. Readers are welcome to comment on the online version of the paper. Correspondence and requests for materials should be addressed to D.H.C. (cobden@uw.edu).